Positive-feedback defines the timing and robustness of angiogenesis

Donna J. Page[1,2], Raphael Thuret[1], Lakshmi Venkatraman[3,4], Tokiharu Takahashi[1], Katie Bentley[3,4,5*], Shane P. Herbert[1,6,*]

[1]Faculty of Biology, Medicine and Health, Michael Smith Building, University of Manchester, Oxford Road, Manchester, M13 9PT, UK.

[2]School of Healthcare Science, Manchester Metropolitan University, Manchester, M1 5GD, UK

[3]Biomedical Engineering Department, Boston University, 610 Commonwealth Avenue, USA, 02215

[4]Immunology, Genetics and Pathology Department, University of Uppsala, 751 85 Uppsala, Sweden.

[5]Center for Vascular Biology Research, Beth Israel Deaconess Medical Center, Harvard Medical School, Boston, Massachusetts 02215, USA.

[6]Lead Contact

*Correspondence: katie.bentley@igp.uu.se (K.B.), shane.herbert@manchester.ac.uk (S.P.H.)

SUMMARY

Blood vessel formation by angiogenesis is critical for tissue development, homeostasis and repair, and is frequently dysregulated in disease[1-3]**. Angiogenesis is triggered by vascular endothelial growth factor receptor-2/3 (VEGFR) signalling, which induces motile endothelial cell (ECs) tip identity**[4,5]**. Tip cells lead new branching vessels, but also coordinate collective EC movement by repressing tip identity in adjacent ECs via Delta-Like 4 (DLL4)-Notch-mediated down-regulation of VEGFR activity**[6-13]**. Hence, angiogenesis is driven by lateral inhibition-mediated competition of ECs for migratory status. Recent work reveals that temporal modulation of this DLL4-Notch-mediated lateral inhibition circuit fundamentally shapes both normal and pathological angiogenesis**[14-17]**. However, the core regulatory network defining the timing and dynamics of EC decision-making is unclear. Here, by integrating computational modeling with *in-vivo* experimentation, we uncover a unique ultrasensitive switch that temporally defines EC lateral inhibition and ultimately determines the timing, magnitude and robustness of angiogenic responses. We reveal that positive-feedback to Vegfr via the atypical tetraspanin, *tm4sf18*, amplifies Vegfr activity and expedites EC decision-making *in-vivo*. Moreover, this Tm4sf18-mediated positive-feedback confers robustness to angiogenesis against changeable environmental conditions by invoking bistable-like behavior. Consequently, mutation of *tm4sf18* in zebrafish delays motile EC selection, generates hypoplastic vessels, sensitizes ECs to fluctuations in pro-angiogenic signal and disrupts angiogenesis. We propose that positive-feedback transforms the normally protracted process of lateral inhibition into a quick, adaptive and robust decision-making mechanism, suggestive of a general framework for temporal modulation of cell fate specification in development and disease.**

RESULTS AND DISCUSSION

Biphasic temporal control of angiogenesis by the Vegfr-Notch axis.

To ensure appropriate angiogenic responses, excessive induction of tip identity is repressed by DLL4-Notch-mediated lateral inhibition[6-13]. During this process, VEGFR activation promotes up-regulation of the Notch ligand DLL4 in emerging tip cells, which *trans*-activates Notch in neighboring cells. Elevated Notch activity promotes down-regulation of VEGFR-2/3 function, rendering laterally-inhibited cells less responsive to VEGF signal (Figure 1A)[6-13]. As such, DLL4-Notch coordinates collective movement of sprouting EC populations, and loss of Notch results in EC hyper-sprouting *in-vivo*. However, we have little-to-no understanding of the underlying temporal features of these decision-making processes. Indeed, lateral inhibition is considered relatively slow, taking upwards of 6 h to complete multiple cycles of gene expression needed to amplify initially small differences in input signal[14,16-19], which is seemingly incompatible with the rapid dynamic changes in EC state, identity and behavior observed in angiogenesis[20,21].

To define the timing of EC decision-making *in-vivo*, we probed the dynamics of lateral inhibition-mediated motile EC selection during zebrafish intersegmental vessel (ISV) angiogenesis. Live-cell imaging of ISV sprouting in *Tg(kdrl:nlsEGFP)*^{zf109} zebrafish embryos revealed that lateral inhibition defines a tight temporally restricted selection window that robustly generated two motile ECs per vessel by 24 hours post fertilisation (hpf; Figure 1B-1C). Importantly, Notch signalling critically closed the window, as in the absence of *dll4* the rate of EC selection did not initially change, but simply continued unstopped (Figure 1C-1D). Unexpectedly, Vegfr levels determined the number of ECs selected within the window, as loss of *flt1* to enhance Vegfr signalling increased the number of ECs selected to sprout, but all were selected within the normal temporal window (Figure 1C). Likewise, the opposite was observed upon brief low-dose inhibition of Vegfr signalling with less cells selected in the time

frame (Figure 1C). As we cannot interrogate the signalling dynamics occurring during the selection time window *in vivo*, we utilized a well validated Memagent-Spring Model (MSM) model of Vegf-Notch selection[22-24] (see Methods). Using unaltered parameters, simulations of perturbation of Vegfr activity generated exactly matching phenomena (Figure S1A-S1C) with a time window (up to timestep 177) in which Vegf-inhibited conditions (vegf=0.038) selected fewer ECs and *flt1* knockdown conditions (Vsink=8) selected more. Monitoring of signalling dynamics in simulations confirmed that Vegf levels determined the number of selected ECs by modulating the speed of selection within this time window.

Importantly, differences in Vegfr-dependent selection rates were not associated with differential EC proliferation (Figure. 1E), although a later switch to Notch-dependent mitosis was revealed by *dll4* knockdown. Moreover, proliferation had minimal effect on overall EC numbers, with both the initial rate of Vegfr-dependent EC induction and Notch-dependent closure of the selection window being the primary determinants of vessel cellularity (Figure 1F). Hence, we reveal that temporal control of angiogenesis is distinctly biphasic, involving (1) Vegfr-level-dependent selection of motile EC numbers, then (2) termination of further selection by Dll4-Notch (Figure 1G).

Positive-feedback temporally regulates lateral inhibition network dynamics

The abrupt switch-like nature of the EC selection window at 24 hpf (Figure. 1C) suggested network ultrasensitivity, whereby a distinct threshold of Vegfr signalling both commits ECs for motile selection and triggers lateral inhibition. Hence, fluctuating Vegfr levels would determine the magnitude of EC selection by dictating how many ECs achieve threshold levels (Figure 1H). Such ultrasensitive responses are frequently driven by positive-feedback loops that amplify signal outputs to promote switch-like dynamics[25,26], but despite the recognized role of Notch-mediated negative-feedback in angiogenesis, the function/identity

of positive-feedback modulators remains elusive. Using our previously validated ordinary differential equation (ODE) mathematical model of DLL4-Notch-mediated lateral inhibition[16], we probed the ability of positive-feedback to modulate the thresholding of EC lateral inhibition. In this model, two adjacent un-patterned ECs compete for selection as either a VEGFR-active DLL4-expressing tip cell or Notch-active laterally inhibited cell using the well-established VEGFR-DLL4-Notch negative-feedback loop (Figure 1I). We created a parameter *P* (see Methods) that creates a positive-feedback interaction whereby VEGFR increases the level/activity of an additional factor that positively feeds back to activate more VEGFR. Using previously defined reaction parameters [16,27-29], we revealed that increasing levels of positive-feedback amplified small differences in VEGFR activity between coupled ECs to drive rapid reciprocal VEGFR/Notch activation, even at low VEGFR levels normally incapable at driving EC sprouting (Figure1J-1K and S1D-S1E). Hence, positive-feedback decreases the threshold of VEGFR activity required to induce motile EC selection and increases the speed of EC decision-making by invoking ultrasensitive switch-like behavior during lateral inhibition.

Vegfr-induced expression of *tm4sf18* promotes positive-feedback

To support *in silico* observations we expanded upon our previous transcriptomic study [30] to identify putative positive-feedback regulators of Vegfr by defining genes transcriptionally activated by Vegfr and repressed by Notch signaling in zebrafish ECs (Figure 2A). Of only 10 candidate Vegfr/Notch-regulated transcripts we identified *h2.0-like homeobox-1* (*hlx1*), a known transcriptional target of Vegfr activity *in-vivo* [30-32] and the atypical tetraspanin *transmembrane 4 L6 family member 18* (*tm4sf18*). TM4SF family proteins are known membrane-associated adaptors that ligand-independently activate receptor tyrosine kinase activity[33,34]. Moreover, *TM4SF1*, the human homologue of *tm4sf18* (Figure S2), is known

to modulate EC motile behavior *in-vitro*[35,36]. Hence, *tm4sf18* represents an ideal candidate positive-feedback modulator of EC motile identity. The highly dynamic nature Vegfr/Notch-regulated expression of *tm4sf18* was validated via qPCR upon inhibition of Vegfr signaling and *dll4* knockdown (Figures 2B-2C), indicating that *tm4sf18* transcription may be tightly restricted to sprouting EC populations (Figure 2D). This was confirmed following characterization of the spatiotemporal pattern of *tm4sf18* expression during zebrafish development. During early ISV sprouting from 22 to 26 hpf, *tm4sf18* expression was almost exclusively restricted to sprouting ISVs (blue brackets in Figure 2E) and was excluded from adjacent non-angiogenic vascular tissues, such as the dorsal aorta (DA). Importantly, the absence of *tm4sf18* in *cloche* (*clo*^{s5}) mutants that lack endothelial tissues [37] confirmed expression in sprouting ECs (Figure 2F). Moreover, *tm4sf18* expression was ectopically expanded to non-angiogenic tissues upon *dll4* knockdown, demonstrating a tight association with EC sprouting potential (Figure 2F). Indeed, rapid repression of *tm4sf18* was observed following fusion of adjacent ISVs to form the dorsolateral anastomotic vessel (DLAV) and subsequent termination of Vegf-induced angiogenic behavior (red brackets in Figure 2E). Hence, expression of *tm4sf18* is dynamically modulated by the Vegfr-Notch axis and is tightly spatiotemporally restricted to sprouting ECs *in-vivo*.

To define *tm4sf18* as a putative temporal modulator of Vegfr/EC signaling *in-vivo*, we used both TALEN and CRISPR/Cas9-mediated gene editing to introduce frame-shift mutations into the long (exon-1) or both long and short (exon-2) isoforms of *tm4fsf18*, respectively (Figure 2G). Importantly, the amplitude of Vegfr signaling in sprouting ECs was unaffected by *tm4sf18* exon-1 and exon-2 mutation (data not shown), indicating that in the absence of Tm4sf18 ECs can still achieve Vegfr activity thresholds sufficient to drive EC motile selection. However, the temporal dynamics of Vegfr signaling were significantly perturbed in homozygous embryos (Figure 2H-2L). To test this, firstly Vegfr activity was fully blocked in

ECs of sprouting ISVs that had already emerged from the dorsal aorta upon incubation of embryos for 3 h with the Vegfr inhibitor, ZM323881. Full disruption of Vegfr activity by ZM323881 was confirmed by a lack of immunoreactivity for pErk (Figure 2I-2L), a well-established readout for Vegfr signaling in sprouting ECs [22,38,39]. Moreover, disruption of pErk was specific to ECs, as levels remained unchanged in neighboring neuronal cells (Figures 2I-2J). Inhibitor was then washed out and recovery of EC pErk levels were monitored over the next 4 h. Quantification of pErk in sprouting tip ECs revealed that normal levels were recovered after just 2 h in both control and *tm4sf18*$^{+/-}$ heterozygous mutant embryos (Figure 2I, 2K). However, recovery of Vegfr-mediated pErk stalled after 1 h of recovery and was significantly disrupted in *tm4sf18*$^{-/-}$ homozygous mutants (Figure 2J, 2L). Hence, consistent with a functional role as a positive-feedback modulator of Vegfr activity, expression of *tm4sf18* amplifies EC signaling *in-vivo* and temporally modulates acquisition of high thresholds of Vegfr-dependent pErk.

Tm4sf18 promotes EC selection and appropriate cellularity of sprouting vessels

To define the functional role of Tm4sf18-mediated positive-feedback in EC decision-making *in-vivo* we quantified the rate of EC selection during ISV sprouting to reveal a significant reduction in *tm4sf18*$^{-/-}$ homozygous embryos (Figure 3A). These observations were consistent with model predictions that in the absence of positive-feedback, fewer ECs achieved the Vegfr selection threshold within a defined selection window (Figure 1J-K, S1D-E). In parallel, we noted that resulting hypocellular ISVs in *tm4sf18*$^{-/-}$ homozygous embryos were often shorter (Figure 3B), an observation that was confirmed upon quantification of EC tip (cell 1) and stalk (cell 2) movement (Figure 3C-3D). This phenotype was reliant on mutation of both short and long Tm4sf18 isoforms, as exon1 homozygous mutant embryos were unaffected (Figure S3A), and was not due to indirect differences in ISV morphology

(Figure S3B). Importantly, disruption of ISV extension did not appear to be a consequence of reduced EC motility, as movement of emerging *tm4sf18*$^{-/-}$ homozygous ECs was initially indistinguishable from wild type and stalling was only observed later in development (Figure 3C-3D). Strikingly, we observed a near-identical phenotype upon disruption of EC proliferation using hydroxyurea/aphidicolin[39,40] (HU/Ap; Figure 3E), suggesting common underlying defects. Although HU/Ap did not disrupt EC motile selection (Figure S3C; unlike loss of *tm4sf18*) and mutation of *tm4sf18* did not disrupt EC proliferation (Figure 3F; unlike HU/Ap) both *tm4sf18* mutation and HU/Ap did generate very similar reductions in ISV cellularity (Figure 3G-3H). Moreover, quantification of tip EC motility in ISVs containing 1, 2 and 3 or more ECs revealed that this cellularity critically determines vessel extension (Figure 3I). Indeed, consistent with the average number of ECs per ISV in *tm4sf18*$^{-/-}$ mutants (approximately two; Figure 3H), ECs lacking Tm4sf18 on average display the normal motility of cells in hypocellular vessels (Figure. 3I). Likewise, wild type and HU/Ap-treated tip ECs display motilities consistent with the average cellularity of vessels in these conditions (Figure S3D). Consequently, both *tm4sf18*$^{-/-}$ mutation and HU/Ap-treatment significantly perturbs migration of ECs to form the DLAV (Figures 3J-3K). Hence, Tm4sf18 modulates lateral inhibition-dependent selection of ECs that critically determines the cellularity of vessels, which in turn determines the rate of extension of sprouting vessels.

Tm4sf18-mediated positive-feedback temporally modulates EC decision-making

Our observations indicated that Tm4sf18 amplifies Vegfr activity to determine the number of ECs that achieve selection threshold. We therefore reasoned that Vegfr inhibition would severely disrupt EC selection in *tm4sf18*$^{-/-}$ homozygous mutants, as ECs would no longer be able to achieve selection threshold in the absence of positive-feedback-mediated amplification of Vegfr signaling. To test this, we blocked EC Vegfr activity with low-dose inhibitor to

putatively force ECs to be reliant on positive-feedback amplification of Vegfr activity. Indeed, upon Vegfr inhibition, not only was the emergence of the first selected ECs now greatly delayed in *tm4sf18*$^{-/-}$ homozygous mutants (Figure 4A-4B), this treatment also generated a large delay to the EC selection window (Figure 4B), independent of any effects on EC proliferation (Figure 4C). Hence, when Vegfr activity is limiting, Tm4sf18-mediated positive-feedback is critical to ensure timely EC selection and temporally defines the dynamics of EC lateral inhibition-mediated EC decision-making.

Positive-feedback generates lateral inhibition network robustness

A core feature of positive-feedback is that it contributes to the establishment of bistable networks, which in turn can confer robustness on cell state transitions by employing hysteresis[25,26]. This reinforces robust cell identity decisions by ensuring that lower input signal levels are required to maintain an active cell state than were needed to drive the initial state transition. Further extension of the ODE modeling revealed that increasing levels of positive-feedback (as provided by Tm4sf18) generated such hysteretic dynamics during Vegfr-Notch-mediated lateral inhibition *in silico* (Figure 4D). However, the range of values that generated bistability was narrow (Figure 4E), which may potentially explain why the temporal dynamics of lateral inhibition are also severely disrupted in *tm4sf18*$^{+/-}$ heterozygous mutants upon Vegfr inhibition (Figure 4B). To test these computational predictions that Tm4sf18-mediated positive-feedback could promote robustness of selected EC identity to variation in inductive signal, we waited until after ECs were selected for branching, i.e. already in ISV sprouts (>22 hpf), and hence already above selection thresholds of Vegfr activity. Then we determined the robustness of signaling to increasing concentrations of Vegfr inhibitor for 3h. In wild type and *tm4sf18*$^{+/-}$ heterozygous embryos, Vegfr signaling was highly robust to partial inhibition of Vegfr, with no significant reduction in pErk levels observed upon

incubation with 40 nM and 80 nM ZM323881 (Figures 4F-4G). In contrast, Vegfr signaling was no longer protected in *tm4sf18*$^{-/-}$ homozygous mutant embryos and pErk levels were significantly disrupted upon incubation of embryos with low dose inhibitor. Hence, as predicted *in silico* (Figure 4D-4E), Tm4sf18-mediated positive-feedback generates signal robustness reminiscent of a bistable network and buffers Vegfr signaling output to maintain robust angiogenic responses, despite fluctuations to input signal (Figure 4H).

Conclusions

Using an integrated *in silico* and *in-vivo* approach we provide evidence that Tm4sf18-mediated positive-feedback generates an ultrasensitive switch that directs the timing and robustness of angiogenesis. Recent work demonstrates that such temporal control of EC lateral inhibition ultimately defines the topology of vascular networks, with faster rates of tip EC selection dramatically increasing vessel network density[14]. As such, it will be critical to determine if Tm4sf18-mediated control of Vegfr activity and lateral inhibition underpin such modulation of vessel branch density in more complex vascular beds. Moreover, observations that positive-feedback confers robustness against fluctuations in Vegfr activity indicates that human *TM4SF* genes may be exploited in therapeutic contexts. For example, abnormally high levels of VEGFR signaling were recently shown to drive synchronous oscillations of Dll4 in neighboring EC, underpinning a switch from normal EC communal branching behavior to the pathological vessel expansion associated with human retinopathies[15]. Disruption of positive-feedback would significantly increase the threshold of VEGFR activity required to switch vessels to abnormal expansion, putatively blocking progression to synchronous oscillatory dynamics and defining a novel therapeutic approach to normalize branching. Likewise, disruption of positive-feedback could increase the potency of existing VEGFR-targeting anti-angiogenic anti-cancer therapeutics by reducing the concentration of compound

required to block functional angiogenesis. This is especially pertinent considering that a key complication of current anti-angiogenic therapeutics is the dose-limiting side-effects encountered with such drugs[40]. Overall, our observations reveal that the relatively slow dynamics of lateral inhibition-mediated cell fate decisions can be transformed into quick, adaptive and robust decision-making processes by simply incorporating positive-feedback. Excitingly, this study suggests a new general mechanism for temporal adaptation of collective cell fate decisions by positive feedback.

Acknowledgements. We thank B. Plusa, R. Das, K. Dorey and members of the Herbert lab for helpful discussion and suggestions. We thank members of the University of Manchester Biological Services Facility for providing excellent fish husbandry. S.P.H. is funded by the Wellcome Trust (Ref. 095718/Z/11/Z), BBSRC (Ref. BB/N013174/1) and BHF (PG/16/2/31863). K.B. is funded by BIDMC and NSF (Ref. 1517390) and the Knut and Alice Wallenberg Foundation. T.T. is funded by the Leverhulme Trust (Ref. RPG-2014-370).

Author contributions. S.P.H. and K.B. conceived the project and designed the experiments. D.J.P. and S.P.H. carried out most of the experiments, while R.T., L.V., T.T. and K.B. carried out some of the experiments. S.P.H., K.B., D.J.P. and R.T. analyzed the data. S.P.H. and K.B. composed the manuscript.

Declaration of interests. The authors declare no competing interests.

Figure Legends

Figure 1. Temporal control of angiogenesis by Vegfr-Notch and positive-feedback. (A) Illustration of the VEGFR-DLL4-Notch lateral inhibition feedback loop between two ECs competing for tip selection. Following lateral inhibition, VEGFR activity increases in cell 2 whereas Notch activity increases in cell 1. (B-F) Time-lapse images of sprouting ISVs in control (B) and *dll4* knockdown (D) *Tg(kdrl:nlsEGFP)*^{zf109} embryos from around 19 hours post-fertilisation (hpf). Brackets indicate dividing cells. Nuclei are pseudocolored. Quantification of the number of ECs selected to branch into ISVs (C), percentage of ECs that undergo proliferation (E) and total number of ECs per ISV (F) in control, *dll4* knockdown, *flt1* knockdown and SU5416-treated embryos. (G) Illustration of the biphasic nature of EC motile selection in control embryos and upon *dll4* or *flt1* knockdown. (H) Putative role of a VEGFR-regulated bipotential switch in modulation of the temporal dynamics of EC motile selection. (I) Outline of the signaling interactions underpinning construction of the 2-cell ODE mathematical model. Blue arrow indicates lateral inhibition between cells. Green and red arrows indicate positive- and negative-feedback via VEGFR, respectively. HE refers to the combined effects of Notch-induced expression of the transcriptional repressors, HES, HEY and HER (see Methods for more details). (J-K) Plots of DLL4 levels in coupled cells following model simulations using varying levels of positive-feedback. Depending on their final level of DLL4, cells were assigned as having acquired either high VEGFR activity and stable tip identity (high levels DLL4; blue arrowhead; J) or high Notch activity and repressed tip identity (low levels DLL4; red arrowhead; K). Blue and red dashed lines represent max and min DLL4 thresholds for stable tip identity and repressed tip identity, respectively. Increasing levels of positive-feedback consistently reduced the threshold of Vegfr activity required for fast tip cell patterning. Error bars: mean ± SEM. *P<0.05, two-way ANOVA test. Scale bars, 25 μm. See also Figure S1.

Figure 2. Tm4sf18 is a positive-feedback modulator of Vegfr signaling dynamics. (A) Fold change in transcript levels of the indicated genes following inhibition of Vegfrs (2.5 µM SU5416), Notch (100 µM DAPT) or both from 22 to 30 hpf. GFP-positive ECs were isolated from inhibitor-treated *Tg(kdrl:nlsEGFP)*^{zf109} embryos by flow cytometry prior to transcriptome profiling. (B) Fold change in *tm4sf18*, *kdrl*, *flt4* and *dll4* transcript levels by qPCR in embryos incubated with SU5416 for the indicated periods of time. SU5416 rapidly down-regulates *tm4sf18* expression. (C) Fold change in *tm4sf18* and *kdrl* transcript levels by qPCR upon *dll4* knockdown. In the absence of Dll4-Notch signaling *tm4sf18* expression was significantly up-regulated. (D) Illustration of proposed regulation of *tm4sf18* expression in sprouting ECs. (E) Lateral views of sprouting intersegmental vessels (ISVs) in *Tg(kdrl:GFP)*^{s843} embryos (left panels) or WT embryos following whole-mount *in situ* hybridization analysis of *tm4sf18* expression (right panels) at the indicated developmental stages (DA, dorsal aorta; DLAV, dorsolateral anastomotic vessel; Blue brackets indicate nascent ISVs; Red brackets indicate anastomosed ISVs; arrows indicate *tm4sf18*-expressing ISVs). (F) Whole-mount *in situ* hybridization analysis of *tm4sf18* expression in *clo*^{s5} mutant embryos or WT embryos upon *dll4* knockdown. (G) Illustration of lesions introduce into the *tm4sf18* genomic loci by TALEN/CRISPR-mediated gene editing. A 19 bp deletion of *tm4sf18* exon 1 and a 16 bp deletion / 2 bp insertion of exon 2 were generated using TALENs and CRISPR/Cas9, respectively. Genomic target sites for the TALENs, gRNA target site and PAM sequence are indicated by blue, red and green highlights, respectively. (H) Strategy for assessing Vegfr signaling dynamics *in-vivo*. Vegfr signaling was first blocked upon incubation of embryos with 0.3 µM ZM323881 for 3 h prior to inhibitor washout for 0, 0.5,1, 2 and 4 h and pErk staining. (I-L) Lateral views of pErk immunostaining in ISV ECs of control (I) or *tm4sf18*$^{-/-}$ homozygous mutant (J) *Tg(kdrl:nlsEGFP)*^{zf109} embryos at 0 and 2 h after inhibitor washout and quantification of pErk fluorescence intensity, in *tm4sf18*$^{+/-}$ heterozygous (K) or

tm4sf18$^{-/-}$ homozygous (L) mutant embryos. Arrowheads in I indicate pErk in neuronal cells. Error bars: mean ± SEM. *P<0.05, two-tailed t test. Scale bars, 100 µm (E) 25 µm (I-J). See also Figure S2.

Figure 3. Tm4sf18 regulates lateral inhibition-mediated selection of motile ECs. (A) Quantification of the number of ECs selected to branch into ISVs of wild-type, *tm4sf18*$^{+/-}$ heterozygous and *tm4sf18*$^{-/-}$ homozygous mutant embryos. (B) Time-lapse images of sprouting ISVs in wild type (B) and *tm4sf18*$^{-/-}$ homozygous mutant (C) *Tg(kdrl:nlsEGFP)*^{zf109} embryos from around 19 hpf. Brackets indicate dividing cells. Nuclei are pseudocolored. (C-E) Quantification of the dorsal movement of tip (cell 1) or stalk (cell 2) ECs in wild type, *tm4sf18*$^{+/-}$ heterozygous mutant (C), *tm4sf18*$^{-/-}$ homozygous mutant (D) or 5-hydroxyurea/aphidocolin (HU/Ap)-treated embryos (E). (F-H) Quantification of the percentage of ECs that undergo proliferation (F), total number of ECs per ISV (G) and distribution of ISV cellularity (H) in wild type, *tm4sf18*$^{+/-}$ heterozygous mutant, *tm4sf18*$^{-/-}$ homozygous mutant and HU/Ap-treated embryos. (I) Quantification of the dorsal movement of tip ECs in ISVs consisting of 1, 2 and 3 or more ECs and comparison with the motility of tip ECs in *tm4sf18*$^{-/-}$ homozygous mutant embryos. (J) Quantification of the number of ECs that reach the DLAV position in wild type, *tm4sf18*$^{+/-}$ heterozygous mutant, *tm4sf18*$^{-/-}$ homozygous mutant and HU/Ap-treated embryos. (K) Illustration of the phenotypic consequences of disrupting EC motile selection or proliferation on ISV extension. Error bars: mean ± SEM. *P<0.05, two-way ANOVA or two-tailed t test. Scale bars, 25 µm. See also Figure S3.

Figure 4. Tm4sf18 defines the timing and robustness of EC decision-making. (A) Time-lapse images of sprouting ISV ECs in either control or *tm4sf18*$^{-/-}$ homozygous mutant *Tg(kdrl:nlsEGFP)*^{zf109} embryos from 20 hpf. Embryos were incubated with 40 nM ZM323881 from 18 hpf onward. Nuclei of sprouting ECs emerging from the DA are pseudocolored. (B-C) Quantification of the number of ECs selected to branch (B) and the percentage of ECs that undergo proliferation (C) in 40 nM ZM323881-treated wild type, *tm4sf18*$^{+/-}$ heterozygous mutant and *tm4sf18*$^{-/-}$ homozygous mutant embryos. (D) ODE modelling of the impact of the level of positive-feedback between Tm4sf18 and VEGF *(P*) on network bistability. When there is no positive-feedback, ECs are not able to switch to an active steady state (high DLL4) even when surrounding VEGF is increased. With increasing *P*, there is a bistable switch in EC state with increasing surrounding VEGF; but at very high *P* values, there is no bistable switch with ECs remaining in an active state with changing VEGF. (E) Two-parameter bifurcation plot with changing VEGF and changing *P* values. Region inside the cusp (i.e. green shaded portion) represents values that are bistable in EC active state with changing values of *P* and VEGF. Everything outside this narrow belt is monostable. (F) Lateral views of sprouting ECs in ISVs of control and *tm4sf18*$^{-/-}$ homozygous mutant *Tg(kdrl:nlsEGFP)*^{zf109} embryos immunostained for pErk. Prior to fixation, embryos were incubated with DMSO or 40 nM ZM323881 from 22 hpf for 3 h. (G) Quantification of pErk fluorescence intensity in wild type, *tm4sf18*$^{+/-}$ heterozygous mutant and *tm4sf18*$^{-/-}$ homozygous mutant embryos following incubation with DMSO and increasing concentrations of ZM323881. Upon *tm4sf18* mutation, Vegfr signaling levels were not robust to subtle Vegfr inhibition. (H) Putative role of positive-feedback-generated hysteretic dynamics in the control of VEGFR signal levels and robustness in angiogenesis. Error bars: mean ± SEM. *P<0.05, two-way ANOVA or two-tailed t test. Scale bars, 25 μm.

Methods

Zebrafish strains and husbandry. Establishment and characterization of the *cloche* (*clo*^{s5}) mutant, *Tg(kdrl:GFP)*^{s843} and *Tg(kdrl:nlsEGFP)*^{zf109} lines have been described elsewhere [37,41,42]. Embryos and adults were maintained under standard laboratory conditions as described previously [22] and were approved by the University of Manchester Ethical Review Board and performed according to UK Home Office regulations.

Time-lapse imaging. Confocal microscopy of live *Tg(kdrl:nlsEGFP)*^{zf109} embryos was performed as previously [22,30]. Briefly, embryos were mounted in 1% low-melt agarose in glass bottom dishes, which were subsequently filled with media supplemented with 0.0045% 1-Phenyl-2-thiourea and 0.1% tricaine. Embryos were imaged using a 20x dipping objectives on a Zeiss LSM 700 confocal microscope. Embryos were maintained at 28°C and stacks were recorded at every 0.3 h. Tracking of cell motility was performed in ImageJ using the manual tracking plugin. All cell tracking recordings were normalized at each time point relative to the position of the dorsal aorta to account for any dorsal or ventral drift of embryos during imaging.

Morpholino oligonucleotide (MO) injections. To knock down gene expression, embryos were injected at the one-cell stage with 5 ng control MO, 5 ng *dll4* MO or 3 ng of *flt1* MO. MO sequences were:

5'- CCTCTTACCTCAGTTACAATTTATA -3' (control)

5'- ATATCGAACATTCTCTTGGTCTTGC – 3' (*flt1)* [43]

5'- GTTCGAGCTTACCGGCCACCCAAAG -3' (*dll4*) [6].

All MOs were purchased from Gene Tools.

Pharmacological treatments. Embryos were manually dechorionated and incubated with compounds from 22 hpf (unless otherwise stated). The following compounds were used in this study: SU5416 (2.5 µM), ZM323881 (40 nM, 80 nM and 160 nM), 5-hydroxyurea (150 µM) and aphidicolin (20 mM).

Model construction & simulation. Interaction between two ECs at the growing end of the angiogenic front have been captured using coupled ordinary differential equations and the 2-cell model previously described [16]. Reactions for the ordinary differential equations of the 2-cell model were written following mass-action kinetics. Details of model construction, list of ODEs, reaction equations and parameters can be found in [16]. Positive-feedback between VEGF and a VEGF-induced/activated factor (*P*) is captured using the equation;

$$V = V * (1 + k_6 * P^n)$$

where k_6 is the positive-feedback rate of *P* production and *n* captures the non-linearity of signaling between VEGF (*V*) sensing and *P*. Model simulations were performed using ODE15s solver in MATLAB2013b (www.mathworks.com). All steady state analysis of the ODE model was carried out using the AUTO bifurcation toolbox in XPPAUT (http://www.math.pitt.edu/~bard/xpp/xpp.html).

Isolation of zebrafish ECs and transcriptome analyses. Flow cytometry-mediated isolation of zebrafish ECs was performed as previously [30]. Briefly, *Tg(kdrl:GFP)*^{s843} embryos were dissected and trunks collected in ice cold Ca^{2+}/Mg^{2+}-free Hank's buffered salt solution (HBSS), washed four times in 1 ml ice cold Ca^{2+}/Mg^{2+}-free HBSS and dissociated in 2 ml TrypLE (Invitrogen) at 27.5° C for 30 min with regular agitation. Dissociation was inactivated upon addition of 100 µl fetal bovine serum (FBS). Dissociated cells were subsequently isolated by centrifugation, re-suspended in 5 ml Ca^{2+}/Mg^{2+}-containing HBSS (with 5% FBS)

and passed through 40 μm filters. ECs were collected upon re-centrifugation of dissociated cells, re-suspension in 0.5 ml Ca^{2+}/Mg^{2+}-containing HBSS (with 5% FBS) and FACS isolation of the *kdrl*:GFP-positive cell population directly into lysis buffer. Total RNA was isolated using the RNAqueous-Micro kit (Ambion). Complementary DNAs were amplified, labeled with Cy3 (from DMSO-treated embryos) or Cy5 (chemical-treated embryos) and hybridized to the Agilent Zebrafish Gene Expression Microarray (V2) by Mogene Lc. The extracted data were normalized and quality controlled using GeneSpring GX software (Agilent). All probes with a green processed signal below 100 were considered as background.

Quantitative real-time PCR (qPCR). Zebrafish embryo or HUVEC cDNA samples were diluted to a concentration of 50 ng/μl with dH_20. Each qPCR reaction was prepared in triplicate in a 48 or 96-well plate with each well consisting of 0.2 μM each forward and reverse primer, 50ng cDNA and SYBR Green Mastermix (Applied Biosystems). Reactions were run on an Eco Real-Time PCR System (Illumina) or Step One Plus Real-time PCR System (Applied Biosystems) alongside negative controls. qPCR data was analyzed by the $\Delta\Delta C_T$ method and expression normalized to *β-actin* and *ef1α* (zebrafish) or *GAPDH* (human). A relative quantification of gene expression was then determined using the formula $2^{-\Delta\Delta CT}$. Primers used for qPCR amplification were:

zebrafish *β actin* forward: 5'-CGAGCTGTCTTCCCATCCA-3'

zebrafish *β actin* reverse: 5'-TCACCAACGTAGCTGTCTTTCTG-3' [44]

zebrafish *dll4* forward: 5'-TGGCCAGTTATCCTGTCTCC-3'

zebrafish *dll4* reverse: 5'-CTCACTGCATCCCTCCAGAC-3' [45]

zebrafish *ef1α* forward: 5'-CTGGAGGCCAGCTCAAACAT-3'

zebrafish *ef1α* reverse: 5'-ATCAAGAAGAGTAGTACCGCTAGCATTAC-3' [44]

zebrafish *flt4* forward: 5'-CTGTCGGATTTGGATTGGGA-3'

zebrafish *flt4* reverse: 5'-GGTGGACTCATAGAAAACCCATTC-3' [46]

zebrafish *kdrl* forward: 5'-ACTTTGAGTGGGAGTTTCATAAGGA-3'

zebrafish *kdrl* reverse: 5'-TTGGACCGGTGTGGTGCTA-3' [46]

zebrafish *tm4sf18* forward: 5'-CTGGATACTGCTTCCTGATCTC-3'

zebrafish *tm4sf18* reverse: 5'-CAAACAGATACCGTCCCTCAT-3'

Cloning of *tm4sf18* and whole-mount *in situ* hybridization. The zebrafish *tm4sf18 in-situ* hybridization construct was generated by PCR amplification of the *tm4sf18* ORF from cDNA and cloning of this fragment into pCR-Blunt II-TOPO (Invitrogen). For probe generation, pCR-Blunt II-TOPO *tm4sf18* was linearized with EcoRV at 37°C for 3 h and T7 was used for transcription. For whole-mount *in situ* hybridization, embryos were fixed in 4% paraformaldehyde (PFA) overnight at 4°C and processed as described previously [47].

Phylogenetic analysis. For phylogenetic analysis of the TM4SF1/4/18 protein family, the NCBI Reference Sequences of TM4SF1, TM4SF4, TM4SF18 proteins of each species were used respectively: human (*Homo sapiens*; NP_055035.1, NP_004608.1, NP_620141.1), mouse (*Mus musculus*; NP_032562.1, NP_663514.2), chicken (*Gallus gallus*; NP_001264407.1, XP_001234023.1, XP_001234069.1), turtle (*Pelodiscus sinensis*; XP_006115992.1, XP_006115993.1, XP_006115991.1), frog (*Xenopus tropicalis*; XP_002937372.1, NP_988958.1, XP_002937374.1), medaka (*Oryzias latipes*; XP_004068091.1, XP_004068090.1), zebrafish (*Danio rerio*; NP_001003489.1, NP_001038487.2), fugu (*Takifugu rubripes*; XP_003974429.1, UniProt H2VCB8), tetraodon (*Tetraodon nigroviridis*; CAF90631.1, CAF90632.1) and elephant shark (*Callorhinchus milii*; XP_007900629.1). Human TM4SF5 protein (NP_003954.2) was used as an out-group for our phylogenetic analysis.

The TM4SF1/4/18 amino acid sequences from all 10 species were aligned using Clustal X2 [48]. The sequences were then manually trimmed of all sites that were not unambiguously aligned. Phylogenetic analysis of amino acid sequences was first performed using NL method implemented in ClustalX2, with outputs displayed using TreeView [49]. Confidence in the phylogeny was assessed by bootstrap re-sampling of the data. For ML tree, the JTT model of protein evolution was used in RAxML [50] with the proportion of invariable sites and gamma parameter estimated from the data, four categories of between-site rate variation; 100 bootstraps were used in the primary ML tree (final ML optimization likelihood: -4945.841564).

Gene editing. TALENs were designed and constructed to target exon 1 of zebrafish *tm4sf18* using online tools (https://tale-nt.cac.cornell.edu/node/add/talen) and as previously described using the Golden Gate method [51]. The target sequences chosen for the forward and reverse TALENs were 5'–TGTGCTCTACAGGATTTGCC-3' and 5'-GCCCTGGTCCCTCTCGCCA-3', respectively. 100 pg of both forward and reverse TALEN mRNA was co-injected into the single cell of zebrafish embryos. At around 24-72 hpf, genomic DNA was extracted from individual embryos and somatic lesions confirmed by high resolution melt (HRM) using Meltdoctor HRM Mastermix (Applied Biosystems) and the following primers:

tm4sf18 TALEN forward 5'-CTGTTTTCTCCCCCACACAC-3'

tm4sf18 TALEN reverse 5'-TACTCACAGCCAGACCACCA-3'

The CRISPR target site within exon 2 of *tm4sf18* (5'-CCTGTGTGTTCCTGGGAATG-3') was identified as previously[52]. gRNA and *nls-zCas9-nls* RNA were generated as previously [53]. 30-100 ng of gRNA and 100-150 ng of *nls-zCas9-nls* RNA were co-injected into single cell stage embryos mixed with a phenol red tracer. At around 24-72 hpf, genomic DNA was

extracted from individual embryos and somatic lesions confirmed by HRM (as above) using the following primers:

tm4sf18 CRISPR forward 5'- CATCAGTCTTTGCAGCGAGA -3'

tm4sf18 CRISPR reverse 5'- TGTAGCATATCCCAACACTCAC -3'

pErk immunostaining. Whole-mount immunostaining for pErk was performed as previously [22]. Briefly, *Tg(kdrl:nlsEGFP)*^{zf109} embryos were fixed in PFA overnight prior to washing in 100% MeOH, incubation with 3% H_20_2 in MeOH on ice for 60 min and further 100% MeOH washes. Embryos were then stored at -20°C for 2 days in MeOH before equilibration with PBT (PBS, 0.1% Tween-20) washes and cryoprotected in 30% sucrose in PBT overnight at 4°C. The next day embryos were equilibrated in PBT, incubated with 150 mM Tris-HCl (pH 9.0) for 5 min and then heated to 70°C for 15 min. Embryos were then washed with PBT and then twice with dH_2O for 5 min. Water was then removed prior to addition of ice-cold acetone for 20 min at -20°C. Acetone was removed prior to PBT washes, one TBST (TBS, 0.1% Tween-20, 0.1% Triton X-100) wash and incubation overnight at 4°C with block solution (TBST, 1% BSA, 10% goat serum). The next day embryos were then incubated with anti-phospho-ERK1/2 antibody (1:250, Cell Signaling; #4370) in blocking buffer overnight at 4°C. Washes in TBST at room temperature were followed by a wash in Maleic buffer (150 mM Maleic acid, 100 mM NaCl, 0.001% Tween-20, pH 7.4) for 30 min. Embryos were then blocked in 2% blocking reagent (Roche) in Maleic buffer for 3 h at room temperature prior to incubation with goat anti-rabbit IgG-HRP (1:1000) in 2% blocking reagent in Maleic buffer overnight at 4°C. Embryos were then washed in Maleic buffer and then PBS at room temperature prior to incubation with 50 µl amplification diluent with 1 µl Tyramide-Cy3 (Perkin Elmer) for 3 h at room temperature in the dark. Embryos were finally washed over

several days in TBST at room temperature. Levels of pErk were quantified as the mean nuclear Cy3 fluorescence intensity using ImageJ.

Statistics. All statistical analyses were performed using GraphPad Prism 6.0 or Microsoft Excel software. Statistical significance was assessed using either unpaired two-tailed Student's *t*-tests or two-way ANOVA tests. Results are presented as mean ± S.E.M. All experiments were repeated at least three times. For all analyses $P<0.05$ was considered statistically significant.

References

[1] Herbert SP, Stainier DYR. Molecular control of endothelial cell behaviour during blood vessel morphogenesis. Nat Rev Mol Cell Biol 2011;12:551–64. doi:10.1038/nrm3176.

[2] Carmeliet P, Jain RK. Molecular mechanisms and clinical applications of angiogenesis. Nature 2011;473:298–307. doi:10.1038/nature10144.

[3] Potente M, Gerhardt H, Carmeliet P. Basic and therapeutic aspects of angiogenesis. Cell 2011;146:873–87. doi:10.1016/j.cell.2011.08.039.

[4] Gerhardt H, Golding M, Fruttiger M, Ruhrberg C, Lundkvist A, Abramsson A, et al. VEGF guides angiogenic sprouting utilizing endothelial tip cell filopodia. J Cell Biol 2003;161:1163–77. doi:10.1083/jcb.200302047.

[5] Ruhrberg C, Gerhardt H, Golding M, Watson R, Ioannidou S, Fujisawa H, et al. Spatially restricted patterning cues provided by heparin-binding VEGF-A control blood vessel branching morphogenesis. Genes Dev 2002;16:2684–98. doi:10.1101/gad.242002.

[6] Siekmann AF, Lawson ND. Notch signalling limits angiogenic cell behaviour in developing zebrafish arteries. Nature 2007;445:781–4. doi:10.1038/nature05577.

[7] Hellström M, Phng L-K, Hofmann JJ, Wallgard E, Coultas L, Lindblom P, et al. Dll4 signalling through Notch1 regulates formation of tip cells during angiogenesis. Nature 2007;445:776–80. doi:10.1038/nature05571.

[8] Leslie JD, Ariza-McNaughton L, Bermange AL, McAdow R, Johnson SL, Lewis J. Endothelial signalling by the Notch ligand Delta-like 4 restricts angiogenesis. Development 2007;134:839–44. doi:10.1242/dev.003244.

[9] Suchting S, Freitas C, le Noble F, Benedito R, Breant C, Duarte A, et al. The Notch ligand Delta-like 4 negatively regulates endothelial tip cell formation and vessel branching. Proceedings of the National Academy of Sciences 2007;104:3225–30. doi:10.1073/pnas.0611177104.

[10] Lobov IB, Renard RA, Papadopoulos N, Gale NW, Thurston G, Yancopoulos GD, et al. Delta-like ligand 4 (Dll4) is induced by VEGF as a negative regulator of angiogenic sprouting. Proc Natl Acad Sci USa 2007;104:3219–24. doi:10.1073/pnas.0611206104.

[11] Benedito R, Rocha SF, Woeste M, Zamykal M, Radtke F, Casanovas O, et al. Notch-dependent VEGFR3 upregulation allows angiogenesis without VEGF-VEGFR2 signalling. Nature 2012;484:110–4. doi:10.1038/nature10908.

[12] Zarkada G, Heinolainen K, Makinen T, Kubota Y, Alitalo K. VEGFR3 does not sustain retinal angiogenesis without VEGFR2. Proceedings of the National Academy of Sciences 2015;112:761–6. doi:10.1073/pnas.1423278112.

[13] Hogan BM, Herpers R, Witte M, Helotera H, Alitalo K, Duckers HJ, et al. Vegfc/Flt4 signalling is suppressed by Dll4 in developing zebrafish intersegmental arteries. Development 2009;136:4001–9. doi:10.1242/dev.039990.

[14] Kur E, Kim J, Tata A, Comin CH, Harrington KI, Costa LDF, et al. Temporal modulation of collective cell behavior controls vascular network topology. Elife 2016;5:a001875. doi:10.7554/eLife.13212.

[15] Ubezio B, Blanco RA, Geudens I, Stanchi F, Mathivet T, Jones ML, et al. Synchronization of endothelial Dll4-Notch dynamics switch blood vessels from branching to expansion. Elife 2016;5:186. doi:10.7554/eLife.12167.

[16] Venkatraman L, Regan ER, Bentley K. Time to Decide? Dynamical Analysis Predicts Partial Tip/Stalk Patterning States Arise during Angiogenesis. PLoS ONE 2016;11:e0166489. doi:10.1371/journal.pone.0166489.

[17] Bentley K, Chakravartula S. The temporal basis of angiogenesis. Philos Trans R Soc Lond, B, Biol Sci 2017;372:20150522. doi:10.1098/rstb.2015.0522.

[18] Matsuda M, Koga M, Woltjen K, Nishida E, Ebisuya M. Synthetic lateral inhibition governs cell-type bifurcation with robust ratios. Nat Commun 2015;6:6195. doi:10.1038/ncomms7195.

[19] Collier JR, Monk NA, Maini PK, Lewis JH. Pattern formation by lateral inhibition with feedback: a mathematical model of delta-notch intercellular signalling. J Theor Biol 1996;183:429–46. doi:10.1006/jtbi.1996.0233.

[20] Jakobsson L, Franco CA, Bentley K, Collins RT, Ponsioen B, Aspalter IM, et al. Endothelial cells dynamically compete for the tip cell position during angiogenic sprouting. Nat Cell Biol 2010;12:943–53. doi:10.1038/ncb2103.

[21] Arima S, Nishiyama K, Ko T, Arima Y, Hakozaki Y, Sugihara K, et al. Angiogenic morphogenesis driven by dynamic and heterogeneous collective endothelial cell movement. Development 2011;138:4763–76. doi:10.1242/dev.068023.

[22] Costa G, Harrington KI, Lovegrove HE, Page DJ, Chakravartula S, Bentley K, et al. Asymmetric division coordinates collective cell migration in angiogenesis. Nat Cell Biol 2016;18:1292–301. doi:10.1038/ncb3443.

[23] Bentley K, Franco CA, Philippides A, Blanco R, Dierkes M, Gebala V, et al. The role of differential VE-cadherin dynamics in cell rearrangement during angiogenesis. Nat Cell Biol 2014;16:309–21. doi:10.1038/ncb2926.

[24] Villefranc JA, Nicoli S, Bentley K, Jeltsch M, Zarkada G, Moore JC, et al. A truncation allele in vascular endothelial growth factor c reveals distinct modes of signaling during lymphatic and vascular development. Development 2013;140:1497–506. doi:10.1242/dev.084152.

[25] Brandman O, Meyer T. Feedback loops shape cellular signals in space and time. Science 2008;322:390–5. doi:10.1126/science.1160617.

[26] Freeman M. Feedback control of intercellular signalling in development. Nature 2000;408:313–9. doi:10.1038/35042500.

[27] Bentley K, Mariggi G, Gerhardt H, Bates PA. Tipping the balance: robustness of tip cell selection, migration and fusion in angiogenesis. PLoS Comput Biol 2009;5:e1000549. doi:10.1371/journal.pcbi.1000549.

[28] Sprinzak D, Lakhanpal A, Lebon L, Santat LA, Fontes ME, Anderson GA, et al. Cis-interactions between Notch and Delta generate mutually exclusive signalling states. Nature 2010;465:86–90. doi:10.1038/nature08959.

[29] Bentley K, Harrington K, Regan E. Can Active Perception Generate Bistability? Heterogeneous Collective Dynamics and Vascular Patterning. Alife 2014:328–35. doi:10.7551/978-0-262-32621-6-ch053.

[30] Herbert SP, Cheung JYM, Stainier DYR. Determination of Endothelial Stalk versus Tip Cell Potential during Angiogenesis by H2.0-like Homeobox-1. Curr Biol 2012;22:1789–94. doi:10.1016/j.cub.2012.07.037.

[31] Sacilotto N, Chouliaras KM, Nikitenko LL, Lu YW, Fritzsche M, Wallace MD, et al. MEF2 transcription factors are key regulators of sprouting angiogenesis. Genes Dev 2016;30:2297–309. doi:10.1101/gad.290619.116.

[32] Fish JE, Gutierrez MC, Dang LT, Khyzha N, Chen Z, Veitch S, et al. Dynamic regulation of VEGF-inducible genes by an ERK-ERG-p300 transcriptional network. Development 2017:dev.146050. doi:10.1242/dev.146050.

[33] Gao H, Chakraborty G, Zhang Z, Akalay I, Gadiya M, Gao Y, et al. Multi-organ Site Metastatic Reactivation Mediated by Non-canonical Discoidin Domain Receptor 1 Signaling. Cell 2016;166:47–62. doi:10.1016/j.cell.2016.06.009.

[34] Jung O, Choi Y-J, Kwak TK, Kang M, Lee M-S, Ryu J, et al. The COOH-terminus of TM4SF5 in hepatoma cell lines regulates c-Src to form invasive protrusions via EGFR

Tyr845 phosphorylation. Biochimica Et Biophysica Acta (BBA) - Molecular Cell Research 2013;1833:629–42. doi:10.1016/j.bbamcr.2012.11.026.

[35] Shih SC, Zukauskas A, Li D, Liu G, Ang LH, Nagy JA, et al. The L6 Protein TM4SF1 Is Critical for Endothelial Cell Function and Tumor Angiogenesis. Cancer Research 2009;69:3272–7. doi:10.1158/0008-5472.CAN-08-4886.

[36] Zukauskas A, Merley A, Li D, Ang L-H, Sciuto TE, Salman S, et al. TM4SF1: a tetraspanin-like protein necessary for nanopodia formation and endothelial cell migration. Angiogenesis 2011;14:345–54. doi:10.1007/s10456-011-9218-0.

[37] Reischauer S, Stone OA, Villasenor A, Chi N, Jin S-W, Martin M, et al. Cloche is a bHLH-PAS transcription factor that drives haemato-vascular specification. Nature 2016;535:294–8. doi:10.1038/nature18614.

[38] Shin M, Beane T, Quillien A, Male I, Zhu LJ, Lawson ND. Vegfa signals through ERK to promote angiogenesis, but not artery differentiation. Development 2016:dev.137919. doi:10.1242/dev.137919.

[39] Nagasawa-Masuda A, Terai K. ERK activation in endothelial cells is a novel marker during neovasculogenesis. Genes Cells 2016. doi:10.1111/gtc.12438.

[40] Loges S, Schmidt T, Carmeliet P. Mechanisms of resistance to anti-angiogenic therapy and development of third-generation anti-angiogenic drug candidates. Genes Cancer 2010;1:12–25. doi:10.1177/1947601909356574.

[41] Jin SW. Cellular and molecular analyses of vascular tube and lumen formation in zebrafish. Development 2005;132:5199–209. doi:10.1242/dev.02087.

[42] Blum Y, Belting H-G, Ellertsdottir E, Herwig L, Lüders F, Affolter M. Complex cell rearrangements during intersegmental vessel sprouting and vessel fusion in the zebrafish embryo. Dev Biol 2008;316:312–22. doi:10.1016/j.ydbio.2008.01.038.

[43] Krueger J, Liu D, Scholz K, Zimmer A, Shi Y, Klein C, et al. Flt1 acts as a negative regulator of tip cell formation and branching morphogenesis in the zebrafish embryo. Development 2011;138:2111–20. doi:10.1242/dev.063933.

[44] Tang R, Dodd A, Lai D, McNabb WC, Love DR. Validation of zebrafish (Danio rerio) reference genes for quantitative real-time RT-PCR normalization. Acta Biochim Biophys Sin (Shanghai) 2007;39:384–90.

[45] Roukens MG, Alloul-Ramdhani M, Baan B, Kobayashi K, Peterson-Maduro J, van Dam H, et al. Control of endothelial sprouting by a Tel-CtBP complex. Nat Cell Biol 2010;12:933–42. doi:10.1038/ncb2096.

[46] Covassin LD, Villefranc JA, Kacergis MC, Weinstein BM, Lawson ND. Distinct genetic interactions between multiple Vegf receptors are required for development of different blood vessel types in zebrafish. Proc Natl Acad Sci USa 2006;103:6554–9. doi:10.1073/pnas.0506886103.

[47] Thisse C, Thisse B. High-resolution in situ hybridization to whole-mount zebrafish embryos. Nat Protoc 2008;3:59–69. doi:10.1038/nprot.2007.514.

[48] Larkin MA, Blackshields G, Brown NP, Chenna R, McGettigan PA, McWilliam H, et al. Clustal W and Clustal X version 2.0. Bioinformatics 2007;23:2947–8. doi:10.1093/bioinformatics/btm404.

[49] Page RD. TreeView: an application to display phylogenetic trees on personal computers. Comput Appl Biosci 1996;12:357–8.

[50] Stamatakis A. RAxML version 8: a tool for phylogenetic analysis and post-analysis of large phylogenies. Bioinformatics 2014;30:1312–3. doi:10.1093/bioinformatics/btu033.

[51] Cermak T, Doyle EL, Christian M, Wang L, Zhang Y, Schmidt C, et al. Efficient design and assembly of custom TALEN and other TAL effector-based constructs for DNA targeting. Nucleic Acids Res 2011;39:e82. doi:10.1093/nar/gkr218.

[52] Ran FA, Hsu PD, Wright J, Agarwala V, Scott DA, Zhang F. Genome engineering using the CRISPR-Cas9 system. Nat Protoc 2013;8:2281–308. doi:10.1038/nprot.2013.143.

[53] Jao L-E, Wente SR, Chen W. Efficient multiplex biallelic zebrafish genome editing using a CRISPR nuclease system. Proceedings of the National Academy of Sciences 2013;110:13904–9. doi:10.1073/pnas.1308335110.

Figure 1

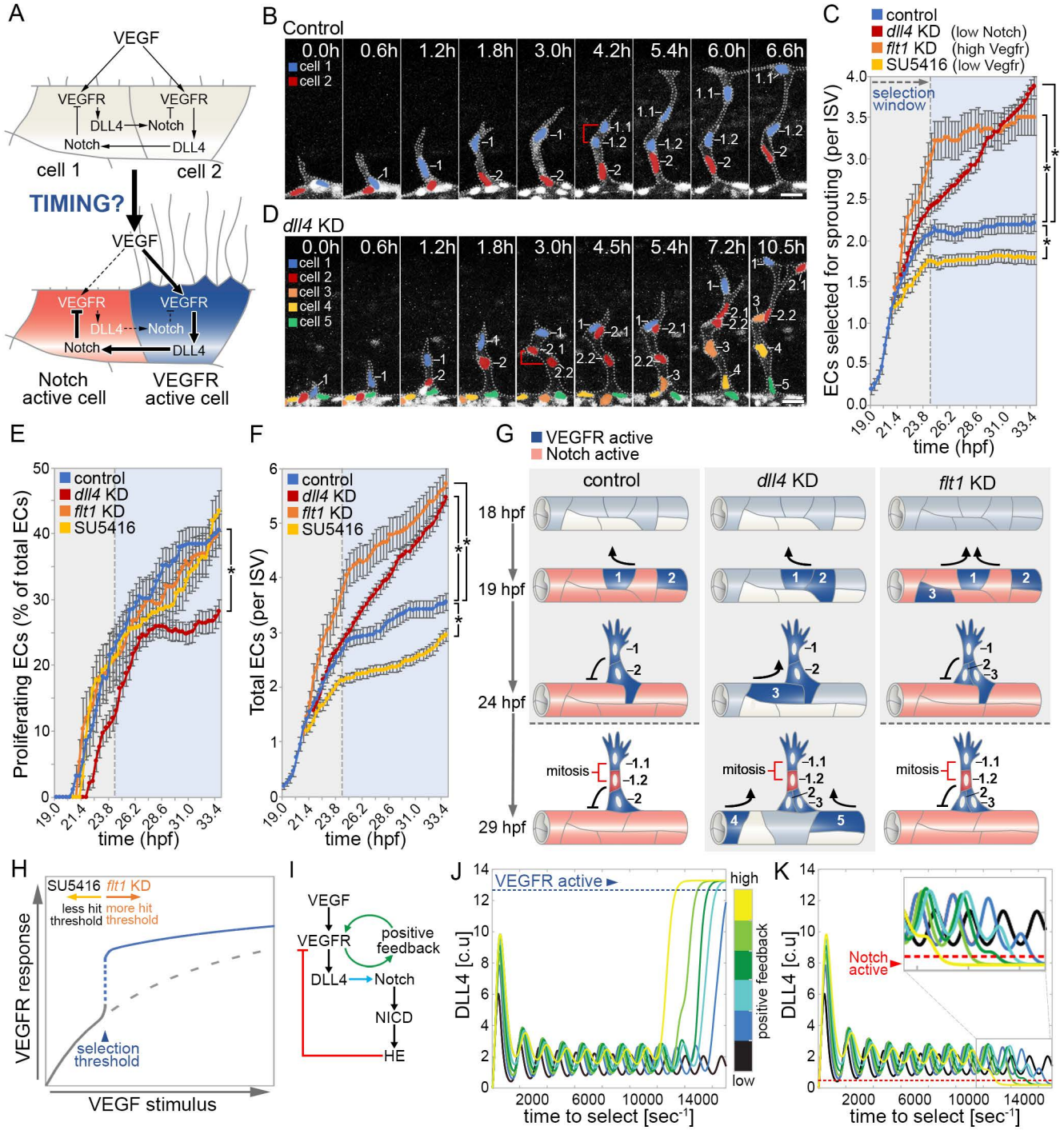
A
VEGF
VEGFR
VEGFR
DLL4
Notch
Notch
DLL4
cell 1
cell 2
TIMING?
VEGF
VEGFR
VEGFR
DLL4
Notch
Notch
DLL4
Notch active cell
VEGFR active cell
B
Control
0.0h 0.6h 1.2h 1.8h 3.0h 4.2h 5.4h 6.0h 6.6h
cell 1
cell 2
D
dll4 KD
0.0h 0.6h 1.2h 1.8h 3.0h 4.5h 5.4h 7.2h 10.5h
cell 1
cell 2
cell 3
cell 4
cell 5
C
control
dll4 KD (low Notch)
flt1 KD (high Vegfr)
SU5416 (low Vegfr)
selection window
ECs selected for sprouting (per ISV)
time (hpf)
E
control
dll4 KD
flt1 KD
SU5416
Proliferating ECs (% of total ECs)
time (hpf)
F
control
dll4 KD
flt1 KD
SU5416
Total ECs (per ISV)
time (hpf)
G
VEGFR active
Notch active
control
dll4 KD
flt1 KD
18 hpf
19 hpf
24 hpf
29 hpf
mitosis
H
SU5416 flt1 KD
less hit threshold
more hit threshold
VEGFR response
selection threshold
VEGF stimulus
I
VEGF
VEGFR
positive feedback
DLL4
Notch
NICD
HE
J
VEGFR active
high
low
positive feedback
DLL4 [c.u]
time to select [sec-1]
K
Notch active
DLL4 [c.u]
time to select [sec-1]

Figure 2

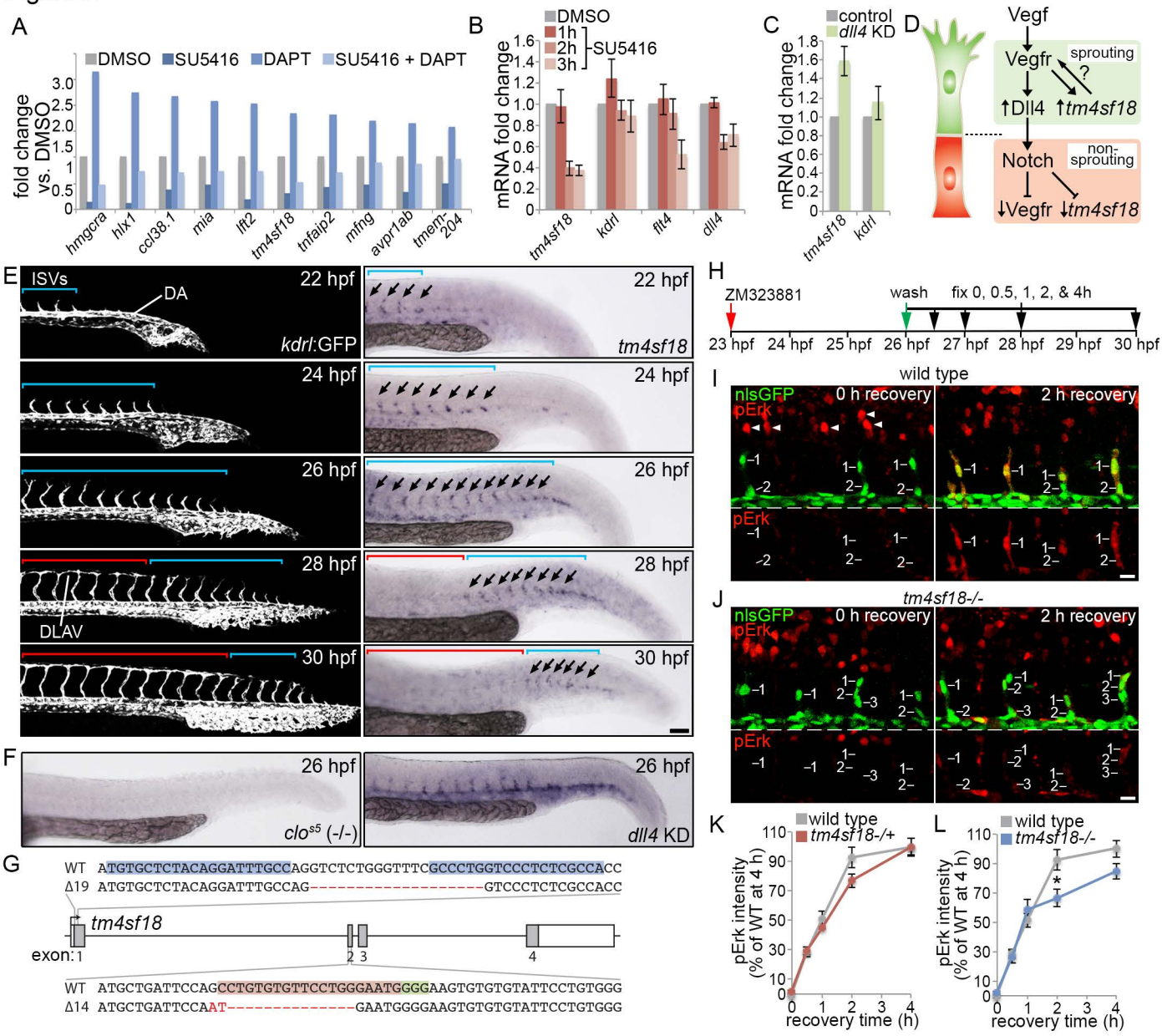
A
DMSO
SU5416
DAPT
SU5416 + DAPT
fold change vs. DMSO
hmgcra
hlx1
ccl38.1
mia
lft2
tm4sf18
tnfaip2
mfng
avpr1ab
tmem-204
B
DMSO
1h
2h
3h
SU5416
mRNA fold change
tm4sf18
kdrl
flt4
dll4
C
control
dll4 KD
mRNA fold change
tm4sf18
kdrl
D
Vegf
Vegfr
sprouting
?
↑Dll4
↑tm4sf18
Notch
non-sprouting
↓Vegfr
↓tm4sf18
E
ISVs
DA
22 hpf
kdrl:GFP
tm4sf18
24 hpf
26 hpf
28 hpf
DLAV
30 hpf
F
26 hpf
clo s5 (-/-)
dll4 KD
G
WT ATGTGCTCTACAGGATTTGCCAGGTCTCTGGGTTTCGCCCTGGTCCCTCTCGCCACC
Δ19 ATGTGCTCTACAGGATTTGCCAG----------GTCCCTCTCGCCACC
tm4sf18
exon: 1 2 3 4
WT ATGCTGATTCCAGCCTGTGTGTTCCTGGGAATGGGGAAGTGTGTGTATTCCTGTGGG
Δ14 ATGCTGATTCCAAT----------GAATGGGGAAGTGTGTGTATTCCTGTGGG
H
ZM323881
wash
fix 0, 0.5, 1, 2, & 4h
23 hpf
24 hpf
25 hpf
26 hpf
27 hpf
28 hpf
29 hpf
30 hpf
I
wild type
nlsGFP
pErk
0 h recovery
2 h recovery
J
tm4sf18-/-
K
wild type
tm4sf18-/+
pErk intensity (% of WT at 4 h)
recovery time (h)
L
wild type
tm4sf18-/-
pErk intensity (% of WT at 4 h)
recovery time (h)

Figure 3

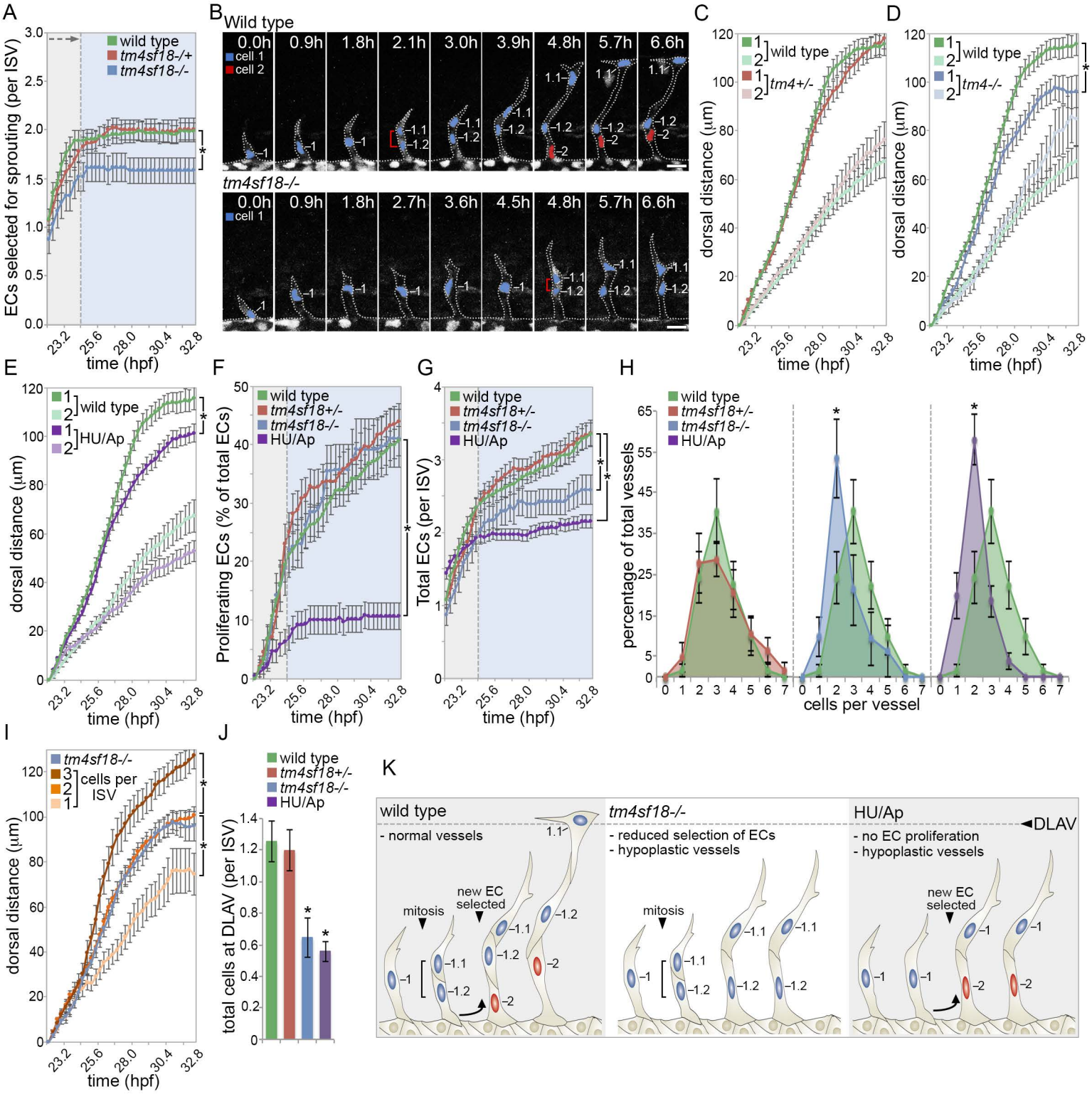
A
ECs selected for sprouting (per ISV)
wild type
tm4sf18-/+
tm4sf18-/-
time (hpf)
B
Wild type
cell 1
cell 2
tm4sf18-/-
C
dorsal distance (µm)
wild type
tm4+/-
D
tm4-/-
E
HU/Ap
F
Proliferating ECs (% of total ECs)
tm4sf18+/-
G
Total ECs (per ISV)
H
percentage of total vessels
cells per vessel
I
cells per ISV
J
total cells at DLAV (per ISV)
K
wild type
- normal vessels
mitosis
new EC selected
tm4sf18-/-
- reduced selection of ECs
- hypoplastic vessels
HU/Ap
- no EC proliferation
- hypoplastic vessels
DLAV

Figure 4

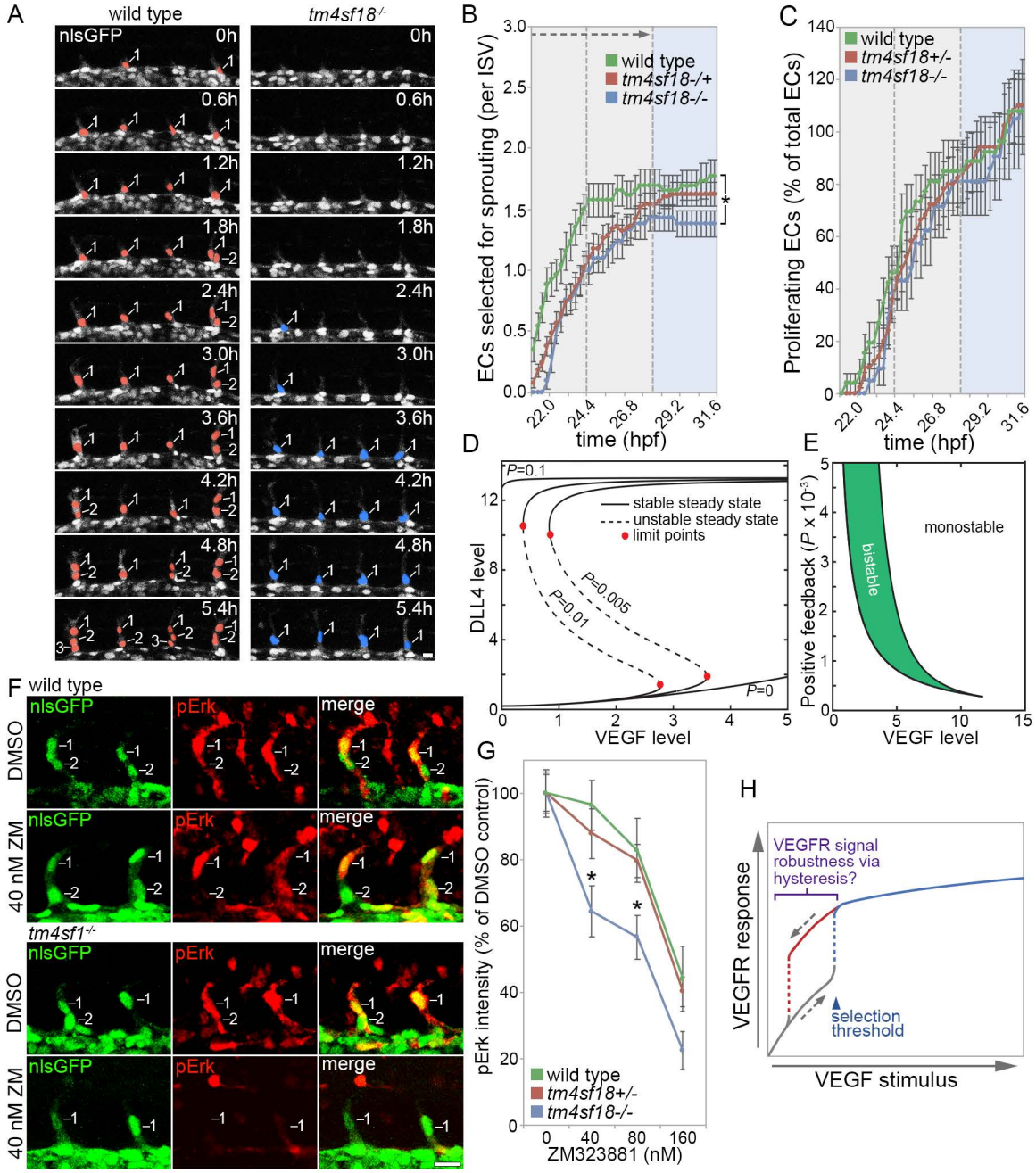
A
wild type
tm4sf18-/-
nlsGFP
0h
0.6h
1.2h
1.8h
2.4h
3.0h
3.6h
4.2h
4.8h
5.4h
B
ECs selected for sprouting (per ISV)
wild type
tm4sf18-/+
tm4sf18-/-
time (hpf)
C
Proliferating ECs (% of total ECs)
wild type
tm4sf18+/-
tm4sf18-/-
time (hpf)
D
P=0.1
stable steady state
unstable steady state
limit points
P=0.005
P=0.01
P=0
DLL4 level
VEGF level
E
Positive feedback (P x 10-3)
monostable
bistable
VEGF level
F
wild type
tm4sf1-/-
DMSO
40 nM ZM
nlsGFP
pErk
merge
G
pErk intensity (% of DMSO control)
wild type
tm4sf18+/-
tm4sf18-/-
ZM323881 (nM)
H
VEGFR signal robustness via hysteresis?
VEGFR response
selection threshold
VEGF stimulus